Synthesis and characterization of CuO/Co_3O_4 and CuO/Fe_2O_3 composites and their potential application in the photocatalytic CO_2 reduction process

Jorge A. Quilantán-Serrano[a], Luis F. Garay-Rodríguez,[b*] Lorena L. Garza-Tovar[a], Leticia M. Torres-Martínez[b,c], I. Juárez-Ramírez[b]

[a]*Universidad Autónoma de Nuevo León, Facultad de Ciencias Químicas, Av. Universidad S/N, Cd. Universitaria, 66455, San Nicolás de los Garza, N. L., México.*
[b]*Universidad Autónoma de Nuevo León, Facultad de Ingeniería Civil - Departamento de Ecomateriales y Energía, Av. Universidad S/N, Cd. Universitaria, 66455, San Nicolás de los Garza, N. L., México.*
[c]*Centro de Investigación en Materiales Avanzados S. C., Miguel de Cervantes 120, Complejo Industrial Chihuahua, 31111, Ch., México.*

*****E-mail de autor responsable: garayr@uanl.edu.mx*

Recibido 15 septiembre 2023, Aceptado 30 septiembre 2023

Abstract
Cupric oxide is a prominent material used as a photocatalyst due to its narrow bandgap; coupling it with other metal oxide semiconductors improves its efficiency due to the favored charge transference. This work reports the synthesis of the composites CuO/Co_3O_4 and CuO/Fe_2O_3, prepared in a sol-gel and hydrothermal two-step methodology to disperse the cocatalyst particles over CuO. The effect of the cocatalyst's concentration over CuO in its structural, optical, and photocatalytic properties was analyzed. A better distribution of the Fe_2O_3 particles over CuO was observed, which resulted in the largest efficiency in the photocatalytic CO_2 reduction to formic acid. Despite this, increasing the cocatalyst concentration reduces the photocatalytic activity due to the surface saturation, probably causing the formation of recombination centers. The presented methodology represents a low-cost way to obtain highly efficient composites in photocatalytic reductive processes.

Palabras clave: Copper oxide, composites, characterization, CO_2 reduction.

1. Introduction

Simple oxide semiconductor materials have attracted attention recently due to their multiple applications thanks to their valuable properties. For that reason, optimizing their synthesis methods and trying to obtain them in lees steps and under low-cost methodologies has been the current challenge for materials scientists.

Cupric oxide is a transition metal oxide with semiconductor properties (p-type) due to its narrow bandgap [1]. Among its properties are superthermal conductivity, stability, antimicrobial activity, and photovoltaic properties [2]; for that reason, it has been used in multiple applications, such as photocatalysis[3], supercapacitors [4], antibacterial surfaces [5], gas sensors[6], chemical absorbers [7], batteries [8], among others.

In this context, different methods have been used to prepare CuO particles, including hydrothermal [9], co-precipitation [10], sol-gel [11], microwave irradiation [12], etcetera, resulting in particles with different structures, allowing it to modify its properties. Sol-gel is a method used to produce solid materials from molecular precursors with the formation of colloidal particles. It has been used to prepare many metal oxide particles, resulting in an easy and low-cost methodology due to the simple equipment used for the particle's preparation.

On the other hand, it is well-known that using composites is favored in different applications compared to using single materials. This is mainly associated with the improved properties achieved with the union of two or more materials with different independent characteristics that add value to the formed material, even more, if both have exhibited good results in a specific application.

In photocatalytic applications, the formation of composites is one of the most used strategies to reduce the recombination of photo-generated charges. Photocatalysis is a process that uses irradiation to activate a semiconductor material, forming electron (e^-) – hole pairs (h^+). In this context, both charged species are responsible for most redox reactions performed on the catalyst's surface. Unfortunately, those charges tend to recombine themselves, reducing the photocatalytic activity.

Co_3O_4 and Fe_2O_3 have been used as cocatalysts forming composites in different photocatalytic processes such as degradation of recalcitrant organic compounds [13, 14], hydrogen production [15, 16], and CO_2 reduction

[17, 18]. In this context, decorating the surface of a base material with both metallic oxides has been responsible for an enhancement in light harvesting, the formation of heterostructures that favors the charge transfer, and in most cases, guide the selectivity of the reaction [19].

Considering the above points, the present work explores the formation of composites of CuO decorated with Co_3O_4 and Fe_2O_3 particles in different concentrations in a two-step sol-gel – hydrothermal synthesis for the CuO and composites preparation, respectively. All the prepared composites were structural and optical characterized, and their potential application was evaluated in the photocatalytic CO_2 reduction reaction to value-added chemicals.

2. Experimental

CuO synthesis

CuO synthesis was performed by the sol-gel methodology. For this purpose, copper acetate (Fermont) was dissolved in isopropyl alcohol and continuously stirred at 70 °C for 1 hour. Subsequently, solvent evaporation was carried out at 90 °C. The recovered powder was thermally treated at 400 °C for one hour in order to achieve phase formation.

Preparation of the composites.

CuO/Co_3O_4 and CuO/Fe_2O_3 composites were prepared following a hydrothermal route. First, Cobalt (II) nitrate hexahydrate (Aldrich) or Iron (III) nitrate nonahydrate (Aldrich) was dissolved in deionized water in an appropriate amount to achieve 1, 5, and 10 wt.% composites. After the complete dissolution, the pH was adjusted to 9 using NH_4OH (DEQ), being added drop to drop. Finally, the CuO prepared in the previous step was suspended in the solutions, and the resulting suspension was transferred to a stainless-steel autoclave to be heat treated at 120 °C for 12 hours. The recovered powders were washed three times with deionized water, dried for 12 hours at 80° C, and stored for later use. For easier reading, the composites will be labeled as follows: Co 1, Co 2, and Co 3 for the CuO/Co_3O_4 composites with 1, 5, and 10 wt.% of Co_3O_4; and F3 1, Fe 2, and Fe 3, for the CuO/Fe_2O_3 composites with 1, 5, and 10 wt.% of Fe_2O_3, respectively.

Characterization.

The structural properties of the prepared composites were analyzed with a Bruker D8 advance XRD, using that information to calculate the crystallite size using the Scherrer equation (Eq. 1):

$$d = \frac{k\lambda}{\beta cos\theta} \quad (1)$$

Where d is the crystallite size in nm, $\boldsymbol{k}$ is the shape factor constant, which is 0.89, $\boldsymbol{\beta}$ is the full width at half maximum in radian, $\boldsymbol{\lambda}$ is the wavelength of the X-ray which is 1.540598 nm, and $\boldsymbol{\theta}$ is the Bragg diffraction angle in radian [20]. The morphological properties were visualized with a JEOL 6490LV SEM. Some HR-TEM analyses were performed in a JEOL 2010 microscope. The diffuse reflectance spectra were collected in a UV-Vis NIR spectrophotometer Cary 5000 coupled with an integration sphere.

Photocatalytic CO_2 reduction reaction.

As a potential application, the prepared composites were evaluated in the photocatalytic CO_2 reduction reaction in aqueous media. 0.1 g of the material was dispersed in 100 mL of deionized water, and the suspension was bubbled with CO_2 for 15 minutes to promote an anoxic media and saturate the system. After that, the reactor was pressurized with 2 psi of CO_2 as the initial concentration and irradiated from the outside with two LED lamps with a maximum emission of 420 nm. At the end of the reaction (3 hours), liquid products were analyzed with gas chromatography (methanol) and liquid chromatography (formic acid and formaldehyde).

3. Results and discussion.

Characterization

Figure 1 summarizes the XDR patterns of bare CuO and the prepared composites. As seen, all the peaks in the bare CuO sample fit with the 00-045-0937 reference with monoclinic crystalline structure and spatial group C2/c, with peaks locate at 32.3, 35.4, 38.6, 48.7, 53.3, 58, 61.5, 65, and 67 degrees of 2 theta, which can be indexed with the (1 1 0), (-1 1 1), (1 1 1), (-2 0 2), (0 2 0), (2 0 2), (-1 1 3), (0 2 2), and (1 1 3) planes, respectively. No additional diffraction peaks were observed, suggesting the formation of a pure CuO phase from the synthesis route. All CuO peaks remained unchanged in position of the patterns obtained for the prepared composites; however, some other reflections were detected. For instance, in the CuO/Co_3O_4 composites (Figure 1a), small peaks at 31, 36, 44, 59, and 65 degrees in 2 theta appeared mainly in Co 2 and Co 3 samples, which are associated to (2 2 0), (3 1 1), (4 0 0), (5 1 1), and (4 4 0) planes of Co_3O_4 (00-043-1003) with cubic crystalline structure (Fd3m). Similarly, in Fe 2 and Fe 3 samples is notorious the presence of peaks at 24, 33, and 57 degrees, belonging to the (0 1 2), (1 0 4), and (0 1 8) planes of 01-089-0598 Fe_2O_3 with rhombohedral structure and R-3c spatial group, being those peaks, in both cases increasing in intensity due to the increase in their concentration. The Crystallite size was also calculated using this data (Table 1). In this context, bare CuO presents a crystallite size of 288 nm, slightly decreasing with incorporation of Co_3O_4 and Fe_2O_3

particles. Conversely, the samples with larger loads of the incorporated cocatalyst particles (Co3 y Fe3) exhibit a slight increase in their average crystallinity. Those results can be associated with the larger presence of Co_3O_4 and Fe_2O_3 phases in the samples, which are more crystalline than CuO. The apparition of the peaks related to the expected phases confirms the formation of the composites and the stability of CuO during the hydrothermal process.

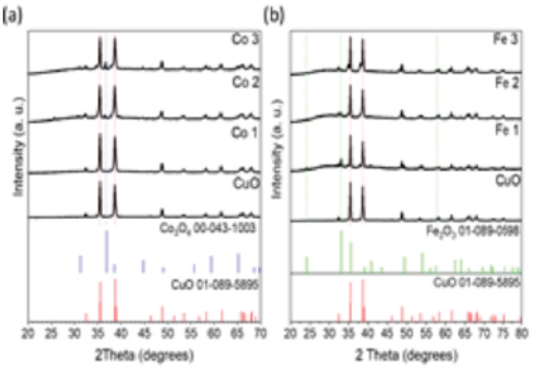

Figure 1. XRD patterns of the prepared composites

Table 1. Summary of the crystallite size and bandgap of the prepared composites.

Sample	Crystallite size (nm)	Bandgap (eV)
CuO	288	2.8
Co 1	214	2.5
Co 2	208	2.1
Co 3	329	2.0
Fe 1	271	1.7
Fe 2	244	1.7
Fe 3	298	1.8

Some micrographs were taken to bare CuO and the composites with larger cocatalyst concentrations (Co3 and Fe3), and those are presented in Figure 2. As seen, bare CuO exhibits an undefined morphology with an average particle size of 900 nm; however, most particles have created agglomerates. As other authors report, this is a common feature of CuO particles synthesized by sol-gel [11].

On the other hand, some differences are observed in the SEM images of the Co 3 and Fe 3 samples. As seen in Figure 2, in both cases, small particles are notorious for covering the surface of others with larger sizes. Despite this, in the case of the Co 3 sample, these smaller particles clump together to form agglomerates, contrary to the Fe 3 sample, where the small particles are well dispersed over the bigger CuO particles.

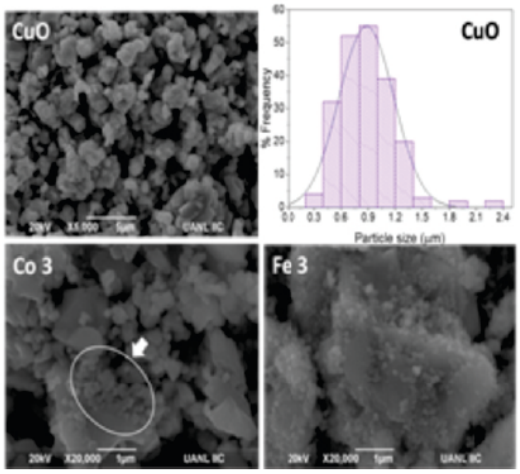

Figure 2. SEM images of the bare CuO and the Co3 and Fe3 composites with the respective particle size distribution of the CuO particles.

This feature is better appreciated in the elemental mapping obtained for both composites. Despite having the same concentration of the metal oxide cocatalysts, Fe seems to be more dispersed, making the CuO on the surface less visible. In contrast, as Co_3O_4 forms agglomerates of large particles, it does not cover all the surface, creating only some zones rich in that element. From these results, it is possible to assume that in the case of Fe_2O_3, the hydrothermal method favored the formation of nanoparticles, contrary to the Co_3O_4.

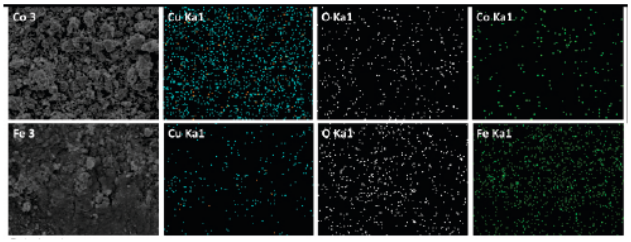

Figure 3. (a) EDS elemental mapping of the Co 3 and Fe 3 composites.

Figure 4 shows the HR-TEM images of the Co 3 and Fe 3 composites. In both images, it is possible to observe the grain boundaries between CuO and the deposited Co_3O_4 and Fe_2O_3 particles, confirming their presence in the composite.

As seen, CuO particles grew in the (1 1 1) face, in concordance with the information obtained in the XRD patterns. A similar behavior is observed in the Co_3O_4 and Fe_2O_3 particles where the (4 0 0) and (1 2 1) planes are observed, confirming the growth of that metallic oxides as cocatalysts.

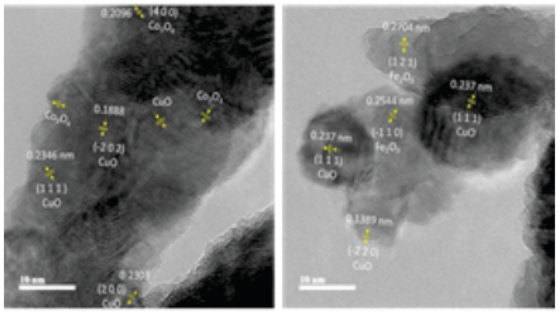

Figure 4. HR-TEM images of the Co 3 and Fe 3 composites.

The absorption spectra of the prepared composites and the bare sample are presented in Figure 5. As can be observed, all the samples exhibit photo-absorption in the visible light zone, suggesting their photo-activation under solar light. This is an expected result due to the coloration of the obtained powders.

On the other hand, comparing the spectra of the composites with the one of CuO, it is possible to observe the apparition of characteristic bands related to the presence of Co_3O_4 and Fe_2O_3. For instance, in the case of the Co composites, a band was remarked between 500 – 800 nm, related to $O^{2-} \rightarrow Co^{3+}$ transition [21], while in the Fe composites, the band in ≈ 540 is associated with $O^{2-} \rightarrow Fe^{3+}$ transition [22].

These data were used to calculate their bandgap energy, summarized in Table 1. As seen, the calculated bandgap value for the CuO sample is 2.8 eV, similar to other reports in the literature [23]. This parameter significantly decreases with the incorporation of both metallic oxide nanoparticles. This change in the bandgap energy can be associated with the good incorporation of both metal oxides forming the composite and the increase in the cocatalyst concentration.

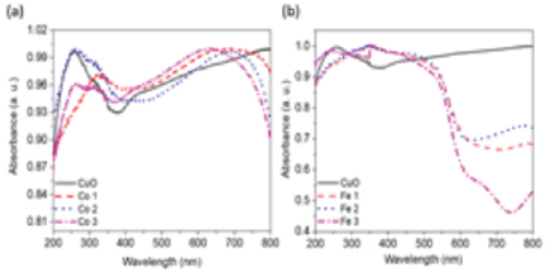

Figure 5. Absorption spectra of the prepared composites.

Photocatalytic CO_2 reduction.

As mentioned in the characterization section, the prepared composites exhibited bandgap values less than 3 eV, which indicates their activation under visible light irradiation. Following this idea, their photocatalytic activation was evaluated in the CO_2 reduction to the value-added chemicals generation.

Figure 6 shows the accumulation of the different products that evolved after three hours of irradiation. It is observed that bare CuO and all the composites present photoactivity, achieving the CO_2 reduction to the formic acid (HCOOH), methanol (CH_3OH), and formaldehyde (HCHO) formation. Control runs were performed without catalyst, illumination, and CO_2, and the lack of products confirms the influence of the photocatalyst's presence in the CO_2 conversion.

As seen, all the samples exhibited selectivity to the formic acid generation, evolving this compound in larger concentration (> 10 µmol; right scale) compared to formaldehyde or methanol (< 1 µmol; left scale). Those results can be associated with the fewer quantity of electrons (e^-) and protons (H^+) required for its formation compared to the other products, according to equations 2 – 4 [24].

$$CO_2 + 2H^+ + 2e^- \rightarrow HCOOH + H_2O \quad (2)$$
$$CO_2 + 4H^+ + 4e^- \rightarrow HCHO + H_2O \quad (3)$$
$$CO_2 + 6H^+ + 6e^- \rightarrow CH_3OH + H_2O \quad (4)$$

Despite this, there was a significant increase in the evolution of all the products with the incorporation of the cocatalysts, compared to bare CuO, which is commonly associated with the well synergistic effect between both materials forming the composite and the efficient electronic transfer achieved.

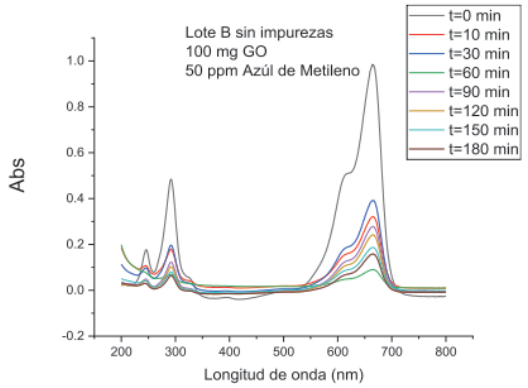

Figure 6. Accumulation of formic acid, formaldehyde, and methanol in the reaction media after three hours of visible-light irradiation.

On the other hand, it can be noticed in the case of all the products that despite the increase in the photocatalytic activity, it reaches a maximum and after it decreases. This behavior can be related to the dispersion of the formed Co_3O_4 or Fe_2O_3 particles over CuO. In this context, according to some reports [25, 26], the saturation of the main photocatalysts surface minimizes the photocatalytic efficiency due to radiation is no longer captured efficiently or particles could act as recombination centers. espite this, an adequate cocatalyst concentration favors the surface properties, and light absorption results in an improved efficiency evolving CO_2 reduction products as the Co 1 and Fe 1 samples.

4. Conclusions

The CuO photocatalytic activity in the CO_2 reduction reaction was improved by forming composites with Co_3O_4 and Fe_2O_3 in a two-step sol-gel and hydrothermal methodology. Their structural characterization confirmed the formation of the expected phases forming the composites in the different cocatalysts concentrations. It was observed that the presence of Co_3O_4 and Fe_2O_4 over the CuO surface decreased its bandgap energy favoring the absorption of visible-light irradiation. Formic acid was evolved as the main CO_2 reduction product, being the samples loaded with the lowest cocatalyst concentration which presented the largest efficiency; mainly associated with the good electronic transference between both metal oxides and CuO. Those results confirm that the formation of composites is a good strategy for obtaining high-efficiency photocatalysts.

5. Acknowledges

Authors thank to CONACYT to financial support through Paradigmas y fronteras de la Ciencia 320379, and UANL through PAICYT 275-CE-2022. We also thank to Dra. Luz Ibarra from CIMAV Monterrey for her valuable help with the HR-TEM measurements.

Author contributions

Jorge A. Quilantán-Serrano: Methodology and investigation, Luis F. Garay-Rodríguez: Conceptualization, writing original draft Lorena L. Garza-Tovar: Conceptualization, methodology, investigation, Leticia M. Torres-Martínez: Resources, writing-review and editing, I. Juárez-Ramírez: Resources, review and editing.

Declaration of competing interests

Authors declare no conflict of interest.

6. References

1. Dhineshbabu NR, Rajendran V, Nithyavathy N, Vetumperumal R, Appl Nanosci,, 2016,6, 933–939.

2. Xu L, Zheng G, Pei S, Wang J, Optik (Stuttg), 2018, 158, 382–390.

3. Raizada P, Sudhaik A, Patial S, et al., Arabian Journal of Chemistry, 2020, 13, 8424–8457.

4. Jagadale SD, Teli AM, Kalake SV, et al, Journal of Electroanalytical Chemistry, 2018, 816, 99–106.

5. Applerot G, Lellouche J, Lipovsky A, et al., Small, 2018, 8, 3326–3337.

6. Kim Y-S, Hwang I-S, Kim S-J, et al., Sens Actuators B Chem, 2008, 135, 298–303.

7. Karthick Kumar S, Suresh S, Murugesan S, Raj SP., Solar Energy, 2013, 94, 299–304.

8. Wang C, Higgins D, Wang F, et al. Nano Energy, 2014, 9, 334–344.

9. Outokesh M, Hosseinpour M, Ahmadi SJ, et al., Ind Eng Chem Res, 2011, 50, 3540–3554.

10. Uma B, Anantharaju KS, Renuka L, et al., Ceram Int, 2021, 47, 10355–10369.

11. Aparna Y, VRK, SSP., Journal of nano- and Electronic Physics, 2012, 4, 030041-03004–5

12. Yang C, Xiao F, Wang J, Su X., Sens Actuators B Chem., 2015, 207, 177–185.

13. Li W, Li W, He K, et al., J Hazard Mater., 2022, 432, 128719.

14. Abdel-Wahab A-M, Al-Shirbini A-S, Mohamed O, Nasr O., J Photochem Photobiol A Chem., 2017, 347, 186–198.

15. Melo MA, Centurion HA, Lucas TTA, et al., ACS Appl Nano Mater, 2020, 3, 9303–9317.

16. Hung W-H, Chien T-M, Tseng C-M., The Journal of Physical Chemistry C, 2014, 118, 12676–12681.

17. Lee D-S, Chen H-J, Chen Y-W., Journal of Physics and Chemistry of Solids, 2012, 73, 661–669.

18. Padervand M, Ghasemi S, Hajiahmadi S, Wang C., Appl Surf Sci, 2021, 544, 148939.

19. Ran J, Jaroniec M, Qiao S-Z, Advanced Materials, 2018, 30, 1704649.

20. Bethi B, Sonawane SH (2018) Nanomaterials and Its Application for Clean Environment. In: Nanomaterials for Green Energy. Elsevier, pp 385–409

21. Garay-Rodríguez LF, Torres-Martínez LM., Journal of Materials Science: Materials in Electronics, 2020, 31, 19248–19265.

22. Suresh R, Sandoval C, Ramírez E, et al., Journal of Materials Science: Materials in Electronics, 2018, 29, 20347–20355.

23. Sagadevan S, Pal K, Chowdhury ZZ., Journal of Materials Science: Materials in Electronics, 2017, 28, 12591–12597.

24. Habisreutinger SN, Schmidt-Mende L, Stolarczyk JK., Angewandte Chemie International Edition, 2013, 52, 7372–7408.

25. Garay-Rodríguez LF, Torres-Martínez LM, Yoshida H, Juárez-Ramírez I., Top Catal., 2022, 65, 1191–1208.

26. Ibarra-Rodriguez LI, Alfaro Cruz MR, Garay-Rodriguez LF, et al., Journal of Materials Research and Technology, 2023, 26, 137–149.